Myocardial Viability Assessment by PET: ^{82}Rb Defect Washout Does Not Predict the Results of Metabolic–Perfusion Mismatch

Mark A. Stankewicz, MD[1]; Craig S. Mansour, MD[1]; Robert L. Eisner, PhD[2]; Keith B. Churchwell, MD[1]; Byron R. Williams, MD[1]; Steven R. Sigman, MD[1]; James Streeter, CNMT[1]; and Randolph E. Patterson, MD[1,2]

[1]Carlyle Fraser Heart Center, Emory Crawford Long Hospital, Division of Cardiology, Department of Medicine, Emory University School of Medicine, Atlanta, Georgia; and [2]Department of Radiology, Emory University School of Medicine, Atlanta, Georgia

PET is a sensitive technique for the identification of viable myocardial tissue in patients with coronary disease. Metabolic assessment with ^{18}F-FDG is considered the gold standard for assessment of viability before surgical revascularization. Prior research has suggested that viability may be assessed with washout of ^{82}Rb between early and late resting images. Our objective was to determine whether assessment of myocardial viability with ^{82}Rb washout is reliable when compared with PET using ^{18}F-FDG. **Methods:** We performed PET for 194 patients referred for PET ^{18}F-FDG/^{82}Rb to assess viability for clinical indications. We included 151 patients with resting defects >10% of the left ventricle (LV) (n = 159 defects). Patients with smaller resting ^{82}Rb defects (<10% LV) were excluded for the purpose of this study. PET images acquired with ^{82}Rb and ^{18}F-FDG defined viability by the mismatch between metabolism and perfusion (^{18}F-FDG >125% of ^{82}Rb uptake in the ^{82}Rb defect). Evidence of viability with ^{82}Rb was assessed by the presence of (i) severity: ^{82}Rb counts in the defect >50% of ^{82}Rb in the normal zone of the resting PET images; (ii) washout: decrease of ^{82}Rb counts in the defect from early to late resting ^{82}Rb images <17% between the first 90-s image and the final 300-s image; or (iii) combined severity and washout criteria, which required positive criteria for (i) and (ii) to indicate viability. **Results:** Prevalence of viability by ^{18}F-FDG/^{82}Rb criteria was 50% (n = 79). Severity criteria yielded a sensitivity of 76% and a specificity of 17%, washout criteria yielded a sensitivity of 81% and a specificity of 23%, and both criteria had a sensitivity of 63% and a specificity of 32%. Positive and negative predictive values were poor for all criteria. No correlation existed between ^{82}Rb washout and ^{18}F-FDG–^{82}Rb mismatch (r^2 = 0.00). Multiple receiver-operating-characteristic plots showed very poor discrimination despite varying criteria for viability by ^{82}Rb (severity from 50% to 60% of normal zone, washout from 12% to 17%). **Conclusion:** ^{82}Rb washout from early to late resting images, combined with quantitative severity of the resting ^{82}Rb defect, did not yield results equivalent to PET ^{18}F-FDG–^{82}Rb mismatch and may not accurately assess myocardial viability.

Received Feb. 17, 2005; revision accepted Jul. 7, 2005.

For correspondence or reprints contact: Randolph E. Patterson, MD, Emory Crawford Long Hospital, 6th Floor Medical Office Tower, Atlanta, GA 30308.
E-mail: randy_patterson@emoryhealthcare.org

Key Words: myocardial viability; ^{82}Rb; PET; coronary artery disease; myocardial perfusion imaging

J Nucl Med 2005; 46:1602–1609

PET has been used as a sensitive technique to assess myocardial tissue viability in patients with coronary artery disease (*1–6*). After a myocardial infarction, overlying surviving tissue may be ischemic (inadequate increment in blood flow during stress), stunned (contractile function temporarily depressed despite restored perfusion after a period of ischemia), or hibernating (contractile function temporarily depressed, possibly an adaptive mechanism against ischemia, which might result from impaired perfusion at rest) (*6–9*). Preserved or absent viability as assessed with ^{18}F-FDG PET has become an important technique because of its ability to predict functional outcome after revascularization of ischemic or hibernating myocardium (*7–9*). Moreover, a flow–metabolism mismatch on ^{18}F-FDG PET has been associated with an elevated risk of subsequent cardiac events in patients treated without revascularization (*10–12*).

PET with ^{82}Rb has been validated for the detection and functional assessment of coronary artery stenoses and infarct size (*13–20*). Previous research has indicated that ^{82}Rb is taken up briefly but clears rapidly from irreversibly injured tissue, but ^{82}Rb is retained in reversibly injured but viable myocardium (*21,22*). Clinical studies followed that compared early and late tracer activity to estimate the rapidity of washout as a method to establish viability. This could result in potential cost savings by avoiding the need for cyclotron-produced ^{18}F-FDG and could avoid close glucose control during ^{18}F-FDG administration (*23,24*).

Our purpose was to evaluate the applicability of ^{82}Rb washout to an unselected clinical population. We defined myocardial viability for this study as the mismatch between ^{18}F-FDG and ^{82}Rb (where ^{18}F-FDG was >125% of ^{82}Rb) and compared this measurement with each of the following 3 ^{82}Rb criteria: (i) severity: ^{82}Rb counts in the defect >50%

of ^{82}Rb in the normal zone of the resting PET images; (ii) washout: decrease of ^{82}Rb counts in the defect from early to late resting ^{82}Rb images <17% between the first 90-s image and the final 300-s image; or (iii) combined severity and washout criteria, which required positive criteria for (i) and (ii) to indicate viability.

MATERIALS AND METHODS

Patient Population

Consecutive patients were referred to Emory Crawford Long Hospital for assessment of viability from August 1993 through June 1996 and from February 2001 through October 2001 and were evaluated for retrospective analysis of their data. We began the analysis with the early (1993–1996) group, but added patients at a later date (2001) to compare results. Protocols and results were the same for these 2 time periods. On the basis of clinical criteria, patients did not undergo ^{18}F-FDG testing if they were found to have a resting defect <5% of the left ventricle (LV) on initial ^{82}Rb imaging and were excluded from the study. After the ^{18}F-FDG study, patients with ^{82}Rb defects <10% of the LV were also excluded because these defects were thought to have limited clinical prognostic significance and the potential for confusion due to proximity of the defect to the adjacent normal tissue. A total of 194 patients were referred for cardiac PET viability assessment. We identified 151 patients with 159 late resting ^{82}Rb defects involving ≥10% of the LV mass (Table 1). Study design and protocols for retrospective data analysis were reviewed and approved by the Institutional Review Board.

Myocardial Imaging Protocol

PET was performed using a Posicam camera (Positron Corp.) producing a 21-slice tomogram with a 125-mm field of view, a spatial resolution of 5–6 mm in the *x*–*y* plane, 10–12 mm in the *z*-axis, with a high sensitivity and counting rate performance. Standard PET image equipment and techniques were used as previously described (*25,26*).

TABLE 1
Study Patient Characteristics

Characteristics	Total *n* = 159*
Age (y)†	62.2 ± 11.4
Sex (male)	116 (74)
Race (Caucasian)	119 (81)
Weight (kg)†	80.4 ± 20.8
Body mass index†	27.0 ± 6.0
LV ejection fraction†	26.9 ± 11.5
Comorbidities	
Diabetes mellitus	49 (31)
Hypertension	51 (32)
Tobacco use (current)	60 (38)
Hypercholesterolemia	65 (41)
Patients with chest pain	97 (61)
Patients with dyspnea	53 (33)
Coronary disease or prior MI	129 (81)
Prior angioplasty	40 (25)
Prior coronary bypass surgery	41 (25)
Family history of coronary disease	83 (52)

*Values in parentheses are percentages.
†Mean ± SD.
MI = myocardial infarction.

Because patients were scheduled for myocardial stress imaging with dipyridamole along with viability assessment, patients were instructed to fast for at least 8 h and to avoid caffeine and theophylline before the test. The patient had an initial pilot or "scout" scan with infusion of 740 MBq ^{82}Rb after continuous elution from the ^{82m}Sr generator. This pilot scan image was used to ensure that the patient's LV was within the 12.5-cm field of view of the camera and to estimate the time required to clear ^{82}Rb from the LV cavity blood pool. In most patients, we waited approximately 80 s after completing the 1-min infusion of ^{82}Rb before beginning acquisition of PET images. In patients with larger LV cavities and slower rates of clearance of ^{82}Rb, we increased the delay time between ^{82}Rb infusion and starting image acquisitions from 80 to as much as 120 s, to allow clearance of ^{82}Rb from the cardiac blood pool. We acquired 2 resting images after infusing 1,480–2,220 MBq ^{82}Rb: the first image (early) for 90 s and the second image (late) for 300 s, beginning as soon as the first image was acquired. Next, we acquired the transmission scan to be used for attenuation correction, beginning 10 min after the first ^{82}Rb infusion and ending just as infusion of dipyridamole was completed (0.142 mg/kg/min for 5 min intravenously). Next, we began infusing ^{82}Rb, 1,480–2,220 MBq intravenously, to match the dose given at rest. We acquired the "stress" ^{82}Rb scan, beginning 6 min after beginning the dipyridamole infusion or after there had been a 10% increase in heart rate or a 10% decrease in blood pressure. When obtained, stress images were not used in the determination of viability. Most patients received aminophylline (75–125 mg intravenously) to reverse side effects of dipyridamole.

Patient preparation for the ^{18}F-FDG imaging included measurements of glucose by a finger prick, before starting the ^{82}Rb study. As previously described (*25*), and based on the initial fasting glucose level, we administered glucose, as 25 g/50 mL (mixed with hydrocortisone [5 mg] to minimize local irritation of the vein). We repeated the serum glucose measurement 30–60 min after the glucose load and administered either regular intravenous insulin or more glucose, as dictated by the glucose level. If necessary, the measurement of glucose and administration of insulin were repeated, to achieve a stable glucose level before administering the ^{18}F-FDG (370 MBq intravenously). We began imaging the heart 60 min after the ^{18}F-FDG was injected.

Image Analysis

The attenuation-corrected tomographic transaxial images, 5-mm thick, were reoriented to vertical long-axis, horizontal long-axis, and short-axis views using the Positron software package. The short-axis views were summarized into polar maps using clinically validated in-house software. Each polar map was quantitated in terms of counts per voxel in each of 1,200 voxels in the LV.

A ^{82}Rb normal file of 50 subjects (25 women, 25 men) with <5% probability of coronary artery disease was previously created (*26*). A normal zone of each patient's LV was defined as the voxels with counts greater than minus 1 SD from the normal file. Each voxel was also defined by its SDs below normal. Count distributions between different regions were compared by quantitation of LV voxels that fell below the mean of the normal file by threshold values of 2.5 SDs. We used a computer program to copy the defect and normal zones on resting ^{82}Rb to the ^{18}F-FDG polar map. These defects were then compared for the difference between count ratios

for the defect zone/normal zone for ^{82}Rb and ^{18}F-FDG in the same defect.

The counts in the defect regions (PDZ = patient's defect zone) were expressed as a percentage of the counts in the normal region (PNZ = patient's normal zone) (Table 2). The severity of the defect was determined by comparison of the average counts per voxel in the defect zone compared with the average counts per voxel in the normal zone in the late resting ^{82}Rb perfusion scan. The late images were used to minimize the influence of background from the LV cavity blood that appears to diminish to a stable low level within 3–4 min after injection (*24*):

$$\text{Defect severity} = \text{PDZ-late/PNZ-late}.$$

The normal region was identified as all pixels with counts greater than minus 1.0 SD from the mean of the normal file, in that region. The "^{82}Rb washout" was calculated as the change in the average count ratios ([PDZ]/[PNZ]) in each region within the defect from early and late images and normalized to the early images using the following formula:

$$^{82}\text{Rb Washout} = (1.0 - [(\text{PDZ-late/PNZ-late})/(\text{PDZ-early/PNZ-early})]) \times 100.$$

This percentage was used as a quantitative assessment of the degree of rubidium "washout" in each region of the resting scan, where a higher percentage represents a faster washout and less evidence of viability. The late resting image SD polar map, mapped to the early resting images, again defined defect and normal zones.

The late rest ^{82}Rb defect and normal zones were mapped to the ^{18}F-FDG polar map, and the ratio of average counts per voxel in the PDZ to average counts per voxel in the PNZ was measured. The ratios were compared to determine whether the defects were matched (^{18}F-FDG $\leq$ ^{82}Rb) or mismatched (^{18}F-FDG $>$ ^{82}Rb). Viability was assessed by the uptake of ^{18}F-FDG within the region of the defect observed on the late ^{82}Rb scan: the relative counts (PDZ/PNZ) in each region within the defect from ^{18}F-FDG and late ^{82}Rb images were determined and compared using the following formula and termed "mismatch":

$$\text{Mismatch} = ([(\text{PDZ } ^{18}\text{F-FDG/PNZ } ^{18}\text{F-FDG})/(\text{PDZ-late/PNZ-late})] - 1.0) \times 100.$$

Mismatch percentage was used as a quantitative assessment of the degree of ^{18}F-FDG–^{82}Rb mismatch in each region, where a higher percentage represents a greater amount of viable myocardium overlying the defect.

To evaluate the effect of background counts, all patients were qualitatively evaluated for LV blood-pool activity on early and late ^{82}Rb images and classified as having a mild, moderate, or severe change (decrease) in LV cavity counts from early to late resting ^{82}Rb images. Those with severe change were considered to have a large background from ^{82}Rb in the LV cavity on early images. In 3 patients from each subgroup, regions of interest (ROIs) were identified on short-axis images, in the following locations: LV cavity, maximum counts in LV myocardium, and minimum counts in LV myocardium. Counts were measured in each region on early and late resting images, and washout was recalculated, correcting for early (CE) and late (CL) background counts:

$$\text{C-Washout} = (1.0 - [(\text{PDZ-late} - \text{CL})/(\text{PNZ-late} - \text{CL})/(\text{PDZ-early} - \text{CE})/(\text{PNZ-early} - \text{CE})]) \times 100.$$

Statistical Analysis

All data analysis was performed using an SPSS statistical software program. Descriptive and frequency information was evaluated by mean, SD, maximum and minimum, and confidence intervals. Distributions were displayed visually by frequency his-

TABLE 2
Definitions of Terms Used in Text

Normal zone	Region of interest (ROI) of LV with ^{82}Rb counts greater than −1.0 SD from the mean of the normal file for those voxels
PDZ-early	Average ^{82}Rb counts measured in patient's defect zone on resting SD polar map in ROI identified by a computer program as those contiguous voxels with counts falling 2.5 or more SDs below the mean of the normal file in this ROI. Early counts are those acquired during the first 90 s.
PDZ-late	Similar to PDZ-early; however, late counts are those acquired in the final 100–300 s of acquisition
PNZ-early	Average ^{82}Rb counts measured in patient's normal zone at rest in ROI identified as those voxels with counts greater than −1.0 SD from the mean of the normal file in this ROI. Early counts are those acquired during the first 90 s.
PNZ-late	Similar to PNZ-early; however, late counts are those acquired in the final 100–300 s of acquisition
Defect severity	$\frac{\text{PDZ-late}}{\text{PNZ-late}}$
^{82}Rb Washout	$(1.0 - [(\text{PDZ-late/PNZ-late})/(\text{PDZ-early/PNZ-early})]) \times 100$
PDZ–^{18}F-FDG	Average ^{18}F-FDG counts in same ROI as the defect identified on resting ^{82}Rb images
PNZ–^{18}F-FDG	Average ^{18}F-FDG counts in same ROI as the normal zone identified on resting ^{82}Rb images
Mismatch	$([(\text{PDZ } ^{18}\text{F-FDG/PNZ } ^{18}\text{F-FDG})/(\text{PDZ-late/PNZ-late})] - 1.0) \times 100$
CE	Average ^{82}Rb background cavity counts measured in LV cavity during the first 90 s of resting acquisition
CL	Average ^{82}Rb background cavity counts measured in LV cavity after the first 90 s of resting acquisition
C-Washout	$(1.0 - [(\text{PDZ-late} - \text{CL})/(\text{PNZ-late} - \text{CL})/(\text{PDZ-early} - \text{CE})/(\text{PNZ-early} - \text{CE})]) \times 100$

tograms. Standard scatter-plot analysis was performed using linear regression analysis and 95% confidence intervals. Sensitivity and specificity was calculated by standard 2 by 2 table evaluation of viability, where the ^{18}F-FDG–^{82}Rb mismatch was considered, for this purpose, to define the presence of viable myocardium. We also varied ^{82}Rb criteria (severity threshold, 0.40–0.65; washout threshold, 12.5%–25%; and combined severity and washout) and ^{18}F-FDG criteria (mismatch >125%, >135%, >145%). A 2-tailed P value of <0.05 was used for statistical significance. Continuous variables are presented as mean ± SD and categoric variables are presented as percentages. To assess whether observed differences were significant, we used χ^2 tests, the Student t test, and ANOVA, requiring a 2-tailed $P < 0.05$ to be considered significant.

RESULTS

One hundred fifty-one patients with 159 defects involving ≥10% of resting LV myocardium were studied (Table 1). There were 74% men, and the average age was 62.2 y. PET ^{18}F-FDG–^{82}Rb mismatch indicated viability in 79 defects (50%), with a mean resting defect size of 29.4% of LV (range, 10%–57%). The mean severity of the resting defects was 0.56 (range, 0.39–0.73), with a mean washout of 12% (range, −18% to 30%).

The severity of ^{82}Rb defect (PDZ/PNZ) showed poor correlation with viability, as measured by ^{18}F-FDG–^{82}Rb mismatch ($r^2 = 0.01$), and washout of ^{82}Rb showed poor correlation with viability by ^{18}F-FDG–^{82}Rb mismatch ($r^2 = 0.00$) (Fig. 1). We also tested whether ^{82}Rb criteria might provide the ability to discriminate viable versus nonviable myocardium, despite limited quantitative correlations with ^{18}F-FDG mismatch. The sensitivity (81%) of ^{82}Rb washout to predict viability by ^{18}F-FDG–^{82}Rb mismatch was reasonable, but the specificity was poor (23%). The positive predictive value (51%) and negative predictive value (56%) were limited. Changing the threshold criteria for ^{82}Rb washout (Fig. 2) did not improve accuracy. We also computed correlations for subgroups of patients to test other factors that might have influenced the study: Patients who had dipyridamole testing ($n = 133$) showed the same poor correlations between ^{82}Rb washout and ^{18}F-FDG–^{82}Rb mismatch ($r^2 = 0.00$) as did patients without dipyridamole testing ($n = 18$) ($r^2 = 0.00$). Also, patients with small- to moderate-sized (10%–29% LV) defects showed similar poor correlations between these 2 variables ($r^2 = 0.00$) as did patients with large (>29% LV) defects ($r^2 = 0.00$).

Similarly, the sensitivity (76%) of ^{82}Rb defect severity to predict ^{18}F-FDG mismatch was reasonable, but poor specificity (17%) limited diagnostic utility (Fig. 3). The positive

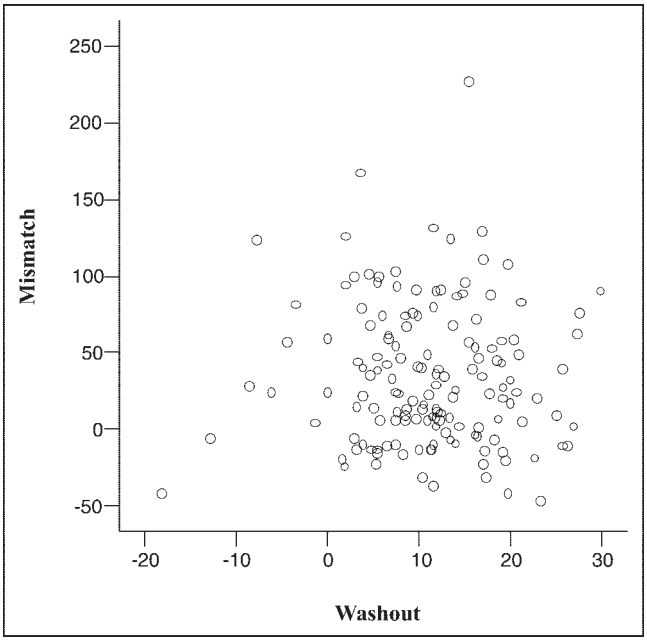

FIGURE 1. Scatterplot shows poor correlation between percentage washout of ^{82}Rb between early and late resting images and percentage mismatch between metabolism (^{18}F-FDG) and perfusion (^{82}Rb uptake) in ^{82}Rb defect used for assessment of viability.

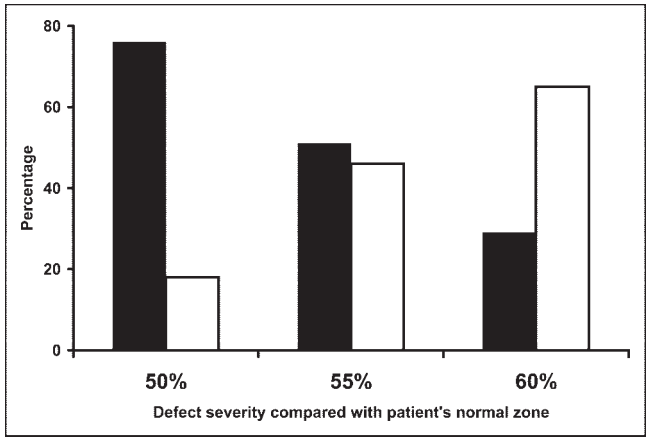

FIGURE 2. Bar graph displays sensitivity (filled bars) and specificity (open bars) of ^{82}Rb defect severity at various cut points when compared with viability using ^{18}F-FDG–^{82}Rb mismatch.

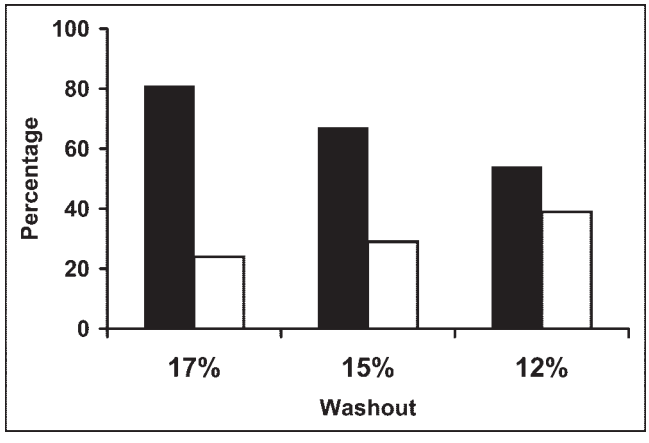

FIGURE 3. Bar graph displays sensitivity (filled bars) and specificity (open bars) of ^{82}Rb defect washout at various cut points when compared with viability using ^{18}F-FDG–^{82}Rb mismatch.

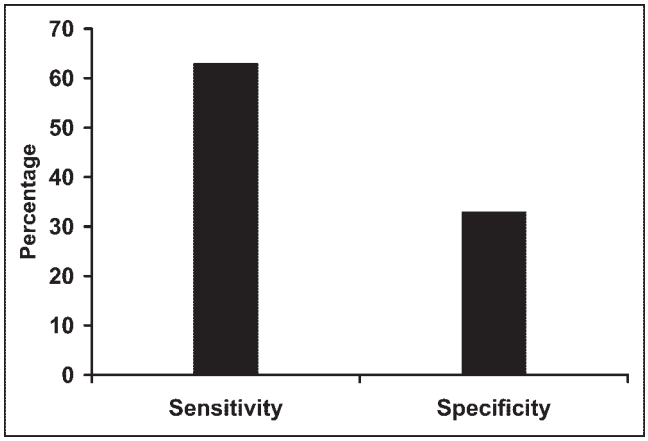

FIGURE 4. Sensitivity and specificity of combined ^{82}Rb severity and mismatch used to define viability when compared with viability assessment using ^{18}F-FDG–^{82}Rb mismatch.

predictive value (48%) and negative predictive value (42%) were limited. Finally, when both defect severity and ^{82}Rb washout were combined, the sensitivity (63%), specificity (32%), positive predictive value (48%), and negative predictive value (47%) indicated limited usefulness (Fig. 4).

Several criteria for viability were evaluated by constructing receiver-operator-characteristic (ROC) curves of false-positive rates (horizontal axis) versus true-positive rates (vertical axis) (Fig. 5). Sensitivity (true-positive rate) and specificity (1 − false-positive rate) were plotted over a wide range of criteria for ^{82}Rb viability (severity, >0.40–0.65; washout, <12.5%–25%), but they provided little ability to discriminate whether a defect would show myocardial viability by ^{18}F-FDG–^{82}Rb mismatch criteria.

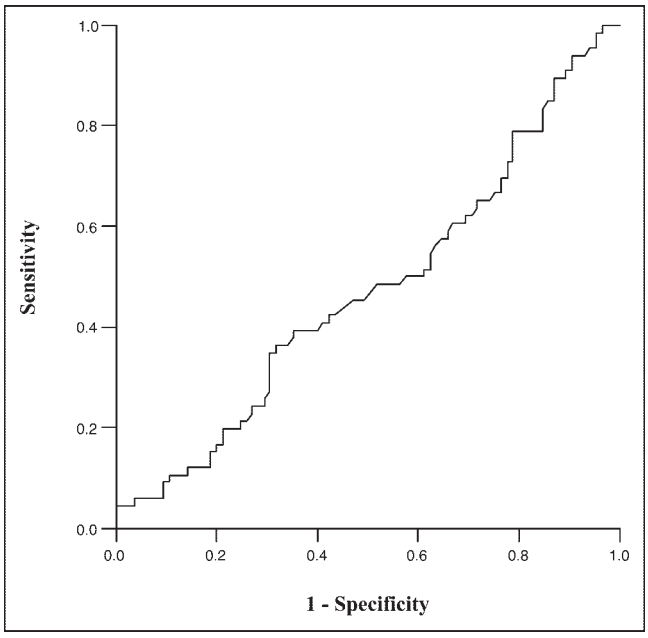

FIGURE 5. ROC curve compares ^{82}Rb washout with ^{18}F-FDG–^{82}Rb.

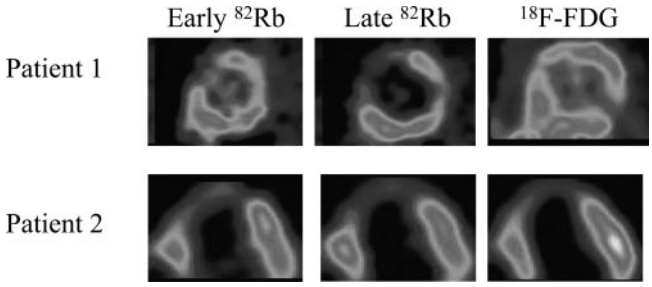

FIGURE 6. Patient 1 (short-axis slices): nonviable by ^{82}Rb washout, viable by ^{18}F-FDG–^{82}Rb. Patient 2 (horizontal long-axis slices): viable by ^{82}Rb washout, nonviable by ^{18}F-FDG–^{82}Rb.

We analyzed a subgroup of 9 patients to assess the impact of background subtraction: 3 from each group having a qualitatively mild, moderate, or severe change in LV cavity counts—that is, background, from early to late resting images. Results suggested that background count subtraction did not change the ^{82}Rb washout results and did not improve the ability of ^{82}Rb defect severity or washout to predict the ^{18}F-FDG–^{82}Rb mismatch. Also, when patients were grouped by background activity, the group with little or no change in background activity between early and late images did not show better correlation between ^{82}Rb washout and ^{18}F-FDG–^{82}Rb mismatch. Finally, after the exclusion of all diabetic patients from the analysis, correlation was not improved ($r^2 = 0.00$).

Figures 6 and 7 show early ^{82}Rb, late ^{82}Rb, and ^{18}F-FDG displays from 2 patients with discrepant ^{82}Rb washout and ^{18}F-FDG viability results. Short-axis slices in the top row (Fig. 6) show a small, mild anterior septal defect on early ^{82}Rb (left image) and a larger, more severe anterior septal defect on late ^{82}Rb (middle image)—with the dramatic washout from early to late suggesting nonviable myocardium. One complication is illustrated in this patient: the high level of background ^{82}Rb in the LV cavity on the early ^{82}Rb image (left) that decreases dramatically on the late ^{82}Rb image (middle). Even this level of background does not seem capable of explaining the magnitude of washout from the myocardial defect. The ^{18}F-FDG images show only a mild defect (right) to indicate a marked mismatch between

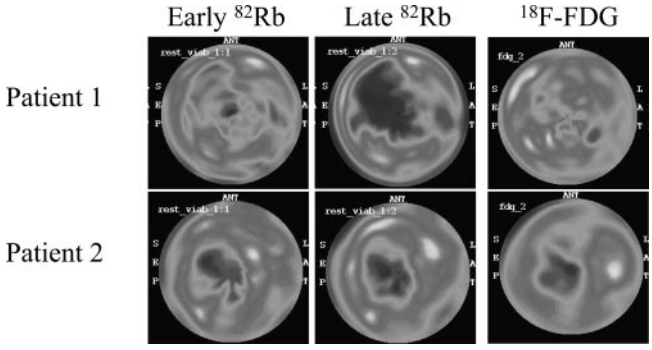

FIGURE 7. Bull's-eye summary views of patients 1 and 2 shown in Figure 6.

the severity of defects on ^{18}F-FDG (mild) and late ^{82}Rb (severe) that indicates viable myocardium. The bottom row shows horizontal long-axis images of one patient during resting acquisitions from left to right: during the early ^{82}Rb acquisition, the late ^{82}Rb, and during the ^{18}F-FDG acquisition. The early ^{82}Rb image (left) shows an apical defect that looks quite similar in severity and size on the late ^{82}Rb image (middle) to suggest viable myocardium, because the ^{82}Rb present early did not wash out very much on late ^{82}Rb images. The ^{18}F-FDG images (right) show a defect that matches the late ^{82}Rb images to indicate nonviable myocardium, because the perfusion (late ^{82}Rb) and metabolic (^{18}F-FDG) scans show closely matched severity and size of defects. These findings are confirmed in the bull's-eye views (Fig. 7).

DISCUSSION

Previous studies (*21,22*) evaluated the retention kinetics of rubidium as a reflection of cell membrane integrity, using a β-detector mounted in a needle and inserted into the myocardium of dogs to measure local β-emissions from ^{82}Rb. On the basis of this work, others (*23,24,27*) proposed using ^{82}Rb instead of ^{18}F-FDG–^{82}Rb mismatch to assess myocardial viability, suggesting that loss of cell membrane integrity, demonstrated by rapid clearance of ^{82}Rb, would parallel the loss of metabolic activity as measured with ^{18}F-FDG. These studies raised the possibility that substantial savings might be possible by ^{82}Rb viability assessment because of the elimination of cyclotron-produced ^{18}F-FDG.

The present study found that PET ^{82}Rb imaging alone could not identify myocardial viability as defined by PET ^{18}F-FDG–^{82}Rb mismatch results. We found no correlation between viability results obtained with ^{82}Rb washout or defect severity and the mismatch between the metabolic tracer ^{18}F-FDG and the flow tracer ^{82}Rb. When, for the purpose of this study, we defined viability as the mismatch between ^{18}F-FDG and ^{82}Rb, the sensitivity, specificity, positive predictive value, and negative predictive value were poor for either resting ^{82}Rb defect severity or washout analysis.

Why did our results differ from these earlier results? Possible reasons include problems with the acquisition of early and late ^{82}Rb images, inaccurate evaluation of the ^{82}Rb washout and severity, and problems with the ^{18}F-FDG results to which ^{82}Rb data were compared. However, the methods used in the current study are in daily use in our laboratory, which has now studied >16,000 patients with ^{82}Rb and >900 patients with ^{18}F-FDG for myocardial viability. The protocols are standardized and consistent with recent guidelines (*25*).

In terms of the ^{82}Rb washout analysis, one critical factor is the time between infusion of ^{82}Rb at rest and beginning the acquisition of the early resting PET images. It is crucial to wait for ^{82}Rb to clear from the blood, because ^{82}Rb counts in the cavity can also scatter into subendocardial defects, making the resting defect appear artificially mild on rest ^{82}Rb, which would suggest ischemia (compared with stress ^{82}Rb) or viability (based on the mildness of the resting defect), or absence of viability (based on marked washout from early myocardial images contaminated by cavitary ^{82}Rb). The time required for clearing ^{82}Rb from the cardiac blood pool is related inversely to the cardiac output and directly to the circulation time. After dipyridamole, the cardiac output increases and the circulation time decreases, so that ^{82}Rb is cleared from the cardiac blood pool more quickly. If background counts could be subtracted accurately, ^{82}Rb blood-pool clearance would not be an issue. Background subtraction, however, is difficult in PET for several reasons. The spatial resolution, measured at full width half maximum, is similar to or larger than the LV wall thickness, rather than being half the value of the object being measured (*28*). Further, drawing a ROI is difficult and the LV cavity is not the only source of background—for example, the background for the subendocardial defects should emphasize LV cavitary ^{82}Rb as background, whereas the normal tissue in the subepicardium should emphasize the different extracardiac sources of background. Even the location of the ROI for background within the LV cavity deserves attention. The results of the analysis of a subgroup of patients suggested that correction for background counts did not change the study results. Further, automated background subtraction, needed for reproducibility and objectivity, does not exist on current commercially used systems.

^{82}Rb defect severity corresponded somewhat more closely with the ^{18}F-FDG–^{82}Rb mismatch than did the washout analysis, but the agreement was still poor. This lack of agreement with severity analysis is harder to explain than the problem with the more complicated washout analysis. A large body of data from animal studies with microsphere measurements after myocardial infarction shows that reduction in average transmural blood flow on a resting study after coronary occlusion correlates with the extent of infarction. This extent of infarction was measured as depletion of myocardial creatine kinase and histologic damage, especially its extension from endocardium to epicardium (*21,22*). Differences between microsphere data and our PET data suggest that the imaging characteristics of the PET camera are the chief factors limiting the ability of this approach to measure viability (*29*), but the extraction fraction of ^{82}Rb, which is somewhat higher in regions with slower flow, may also contribute to this problem (*30*).

In the present analysis, we defined the defects with greater resolution and reproducibility than in the other studies cited by using a polar ("bull's-eye") map of the defect. This map used an automated computer program with clearly defined criteria to determine the percentage of the LV voxels that were abnormal, based on their having counts reduced by 2.5 or more SDs below the average of the normal file. Thus, it was not necessary to introduce new sources of error when using either ROIs defined by an observer or arbitrarily drawn segments that are less likely to

correspond to anatomic vascular distribution. Analysis of arbitrarily assigned segments, as done in prior studies, inevitably leads to sampling a mixture of normal and abnormal myocardium within most segments. The identification of perfusion defects by objective criteria written into a computer program allows unambiguous, reproducible definition of an abnormal region (*25*).

For a technique to gain widespread acceptance, it should be easy to use and widely applicable to a variety of clinical environments and populations. Our study suggests that ^{82}Rb washout used in a "real-world" setting yields results that differ considerably from ^{18}F-FDG–^{82}Rb mismatch. It is possible that the larger and unselected patient population in our study provided a broader basis for comparison with the general population. Our only patient selection criterion was referral by a cardiologist or cardiac surgeon for viability assessment and that they showed a resting perfusion defect that reduced counts by >2.5 SDs, and occupied >10% LV mass, so that milder defects (22% of patients initially referred) were excluded. It is possible that other studies have included some patients with milder, smaller defects that would not be most relevant to clinical decisions regarding revascularization and viability.

Alternatively, if drawing the defect ROI led to smaller defects with uniform severity by avoiding the edge of the defect, then the defects might have appeared somewhat smaller but more severe. We examined these effects by comparing automatically defined defects that were small or moderate (≤29% LV, $n = 81$) versus large (>29% LV, $n = 78$), based on a median defect size of 29% LV. There was no difference in the correlation between ^{82}Rb washout and ^{18}F-FDG–^{82}Rb mismatch based on small or moderate defect size ($r^2 = 0.00$) versus large defect size ($r^2 = 0.00$), suggesting that the conclusion of the present study was not determined by potential artifacts arising from the partial-volume effect and differences in defect size (*28*). The performance of ^{82}Rb stress myocardial perfusion imaging is also a consideration. Although it is recognized that regional ^{18}F-FDG uptake may be affected by prolonged metabolic effects of any stress-induced ischemia, stress-induced ischemia during persantine stress is uncommon and, therefore, unlikely to alter the overall findings of this study.

The lack of correlation between the numeric indices of viability obtained with ^{82}Rb washout and ^{18}F-FDG–^{82}Rb mismatch does not necessarily mean that resting ^{82}Rb cannot predict other useful clinical information. It is troubling for clinical applications, however, that ^{82}Rb severity or washout criteria were not able to discriminate the presence or absence of viable myocardium, as described by their sensitivities and specificities, compared with the ^{18}F-FDG–^{82}Rb mismatch. Because the 2 techniques do not produce similar viability assessments, more study is necessary to establish which method is better able to predict subsequent events, such as clinical outcomes or changes in cardiac function after revascularization. PET with perfusion and metabolism of ^{18}F-FDG has been validated to correlate with return of myocardial function after revascularization.

CONCLUSION

These results show that resting ^{82}Rb imaging results, analyzed for defect severity or washout, differ from the assessment offered by ^{18}F-FDG–^{82}Rb mismatch. This study suggests caution in using ^{82}Rb alone as a measure of myocardial viability. Further study of ^{82}Rb is needed to assess the ability of ^{82}Rb to predict outcomes after revascularization.

ACKNOWLEDGMENTS

The authors thank our patients, the PET center nursing and technologist staff, the Cardiology physician staff, and our referring physicians. Carlyle Fraser Heart Center (Atlanta, GA) and Positron Corp. Inc. (Houston, TX) provided financial support.

REFERENCES

1. Marshall RC, Tillisch JH, Phelps ME, et al. Identification and differentiation of resting myocardial ischemia in man with positron computed tomography, ^{18}F-labeled fluorodeoxyglucose, and N-13 ammonia. *Circulation.* 1983;67:766–778.
2. Camici P, Araujo L, Spinks T, Lammertsma AA, Jones T, Maseri A. Myocardial glucose utilization in ischemic heart disease: preliminary results with F18-fluorodeoxyglucose and positron emission tomography. *Eur Heart J.* 1986;7:19–23.
3. Brunken RC, Schwaiger M, Grover-McKay M, et al. Positron emission tomography detects tissue metabolic activity in myocardial segments with persistent thallium perfusion defects. *J Am Coll Cardiol.* 1987;10:557–567.
4. Schwaiger M, Brunken RC, Krivokapich J, et al. Beneficial effect of residual anterograde flow on tissue viability as assessed by positron emission tomography in patients with myocardial infarction. *Eur Heart J.* 1987;8:981–988.
5. Gropler RJ, Siegel BA, Sampathkumaran K, et al. Dependence of recovery of contractile function on maintenance of oxidative metabolism after myocardial infarction. *J Am Coll Cardiol.* 1992;19:989–997.
6. Klocke FJ, Baird MG, Bateman TM, et al., eds. ACC/AHA/ASNC Guidelines for the Clinical Use of Cardiac Radionucleotide Imaging. Available at: http://www.acc.org/clinical/guidelines/radio/nri_fulltext.pdf. Accessed September 22, 2004.
7. Tillisch J, Brinken R, Marshall R, et al. Reversibility of cardiac wall motion abnormalities predicted by positron tomography. *N Engl J Med.* 1996;314:884–888.
8. Bonow RO, Dilsizian V, Cuocolo A, et al. Identification of viable myocardium in patients with chronic coronary artery disease and left ventricular dysfunction and PET imaging with 18-F-florodeoxyglucose. *Circulation.* 1991;83:26–37.
9. Marwick TH, MacIntyre WJ, Lafont A, et al. Metabolic responses of hibernating and infarcted myocardium to revascularization: a follow-up study of regional perfusion, function, and metabolism. *Circulation.* 1992;85:1347–1353.
10. Eitzman D, Al-Aouar ZR, Kanter HL, et al. Clinical outcome of patients with advanced coronary artery disease after viability studies with positron emission tomography. *J Am Coll Cardiol.* 1992;20:559–565.
11. Tamaki N, Kawamoto M, Takahashi N, et al. Prognostic value of an increase in fluorine-18 deoxyglucose uptake in patients with myocardial infarction: comparison with stress thallium imaging. *J Am Coll Cardiol.* 1993;22:1621–1627.
12. DiCarli MF, Davidson M, Little R, et al. Value of metabolic imaging with positron emission tomography for evaluating prognosis in patients with coronary artery disease and left ventricular dysfunction. *Am J Cardiol.* 1994;73:527–533.
13. Goldstein R, Mullani N, Wong W, et al. Positron imaging of myocardial infarction with rubidium-82. *J Nucl Med.* 1986;27:1824–1829.
14. Gould K, Goldstein R, Mullani N, et al. Noninvasive assessment of coronary stenoses by myocardial perfusion imaging during pharmacologic coronary vasodilation. VIII. Clinical feasibility of positron cardiac imaging without a cyclotron using generator-produced rubidium-82. *J Am Cardiol.* 1986;7:775–789.
15. Gould KL. Identifying and measuring severity of coronary artery stenosis: quantitative coronary arteriography and positron emission tomography. *Circulation.* 1988;78:237–245.

16. Gould K, Goldstein R, Mullani N, et al. Clinical feasibility, sensitivity and specificity of positron cardiac imaging without a cyclotron using generator produced Rb-82 for the diagnosis of coronary artery disease [abstract]. *J Nucl Med.* 1986;27(suppl):P976.
17. Demer L, Gould K, Goldstein R, et al. Assessment of coronary artery disease severity by positron emission tomography: comparison with quantitative arteriography in 193 patients. *Circulation.* 1989;79:825–835.
18. Go RT, Marwick TH, MacIntyre WJ, et al. A prospective comparison of rubidium-82 PET and thallium-201 SPECT myocardial perfusion imaging utilizing a single dipyridamole stress in the diagnosis of coronary artery disease. *J Nucl Med.* 990;31:1899–1905.
19. Marwick TH, MacIntyre WJ, Salcedo EE, et al. Identification of ischemic and hibernating myocardium: feasibility of post-exercise F-18 deoxyglucose positron emission tomography. *Cathet Cardiovasc Diagn.* 1991;22:100–106.
20. Stewart RE, Schwaiger M, Molina E, et al. Comparison of rubidium-82 positron emission tomography and thallium-201 SPECT imaging for detection of coronary artery disease. *Am J Cardiol.* 1991;67:1303–1310.
21. Goldstein R. Kinetics of rubidium-82 after coronary occlusion and reperfusion: assessment of patency and viability in open-chested dogs. *J Clin Invest.* 1985; 75:1131–1137.
22. Goldstein RA. Rubidium-82 kinetics after coronary occlusion: temporal relation of net myocardial accumulation and viability in open-chested dogs. *J Nucl Med.* 1986;27:1456–1461.
23. Gould KL, Yoshida K, Hess MJ, et al. Myocardial metabolism of fluorodeoxyglucose compared to cell membrane integrity for the potassium analogue rubidium-82 for assessing infarct size in man by PET. *J Nucl Med.* 1991;32: 1–9.
24. vom Dahl J, Muzik O, Wolfe ER, et al. Myocardial rubidium-82 tissue kinetics assessed by dynamic positron emission tomography as a marker of myocardial cell membrane integrity and viability. *Circulation.* 1996;93:238–244.
25. Bacharach SL, Bax JJ, Case J, et al. PET myocardial glucose metabolism and perfusion imaging. Part 1. Guidelines for data acquisition and patient preparation. *J Nucl Cardiol.* 2003;10:543–556.
26. Patterson RE, Horowitz SF, Eisner RL. Comparison of modalities to diagnose coronary artery disease. *Semin Nucl Med.* 1994;24:286–310.
27. Go RT, Macintyre WJ, Saha GB, et al. Hibernating myocardium versus scar: severity of irreversible decreased myocardial perfusion in prediction of tissue viability. *Radiology.* 1995;194:151–155.
28. Sorensen JA, Phelps ME. *Physics in Nuclear Medicine.* Philadelphia, PA: WB Saunders; 1987:406–408.
29. Basingthwaite JB. Flow estimation from tracer washout. *Prog Cardiovasc Dis.* 1977;20:83–107.
30. Mullani NA, Goldstein RA, Gould KL, et al. Myocardial perfusion with rubidium-82: measurement of extraction fraction and flow with external detectors. *J Nucl Med.* 1983;24:898–906.